PERFORMANCE ENHANCEMENT OF WIND ENERGY CONVERSION SYSTEMS USING PMSG WITH BACKSTEPPING AND ANN-BASED MPPT CONTROL

Wassila Hattab[1], Abdelhamid Benakcha[2], Seddik Tabet[3], Amira Slimani[4]

[1,2,3,4] dept. Electrical Engineering-LGEB Lab, Biskra University Biskra, Algeria

[1]http://orcid.org/0009-0004-7004-5092 , [2]http://orcid.org/0000-0003-4462-7676 , [3]http://orcid.org/0000-0003-4835-2067 ,
[4]http://orcid.org/0009-0009-3259-5743

Email: wassila.hattab@univ-biskra.dz , abdelhamid.benakcha@univ-biskra.dz , seddik.thabet@univ-biskra.dz, amira.slimani@univ-biskra.dz

ARTICLE INFO

ABSTRACT

This paper investigates the performance enhancement of wind energy conversion systems (WECS) using a Permanent Magnet Synchronous Generator (PMSG) specifically designed for standalone, fixed-pitch, variable-speed wind turbines. The study focuses on controlling the PMSG using Backstepping control which enables Maximum Power Point Tracking (MPPT) using the Tip Speed Ratio (TSR) method. Initially, a Proportional-Integral (PI) controller was implemented for regulating the generator speed. However, this approach encountered significant limitations, particularly in managing speed overshoot and responsiveness under fluctuating wind conditions. To address these issues, a neural network controller was introduced as a replacement for the conventional PI controller. This neural network controller provides an adaptive control mechanism capable of dynamically adjusting to change, thereby eliminating overshoot and greatly enhancing response speed and overall system stability. This work provides a reliable and efficient control solution where was the proposed control strategy was rigorously evaluated through numerical simulations in Matlab/Simulink, which confirmed its ability to stabilize the system and achieving both steady-state and dynamic optimization of wind energy conversion systems.

I. INTRODUCTION

With the rising global focus on sustainable and environmentally friendly electricity generation, many countries have increasingly turned to renewable energy sources [1]. Currently, approximately 38% of global electricity production is derived from renewable sources, marking a shift aimed at drastically reducing carbon emissions [2], [3]. Among the various renewable technologies, wind energy stands out as one of the promising solutions [4], [5]. According to the latest data from the International Renewable Energy Agency, about 27% of renewable energy-generated electricity, or 825 GW, comes from wind energy, a figure projected to reach 1756 GW by 2030 [6]. As wind energy systems evolve, variable-speed wind turbine (VSWT) technology has gained popularity over fixed-speed systems due to its efficiency and flexibility in adapting to change wind conditions [7]. In particular, wind turbines based on (PMSM) have proven highly

effective and dependable for transforming wind energy into electrical power, positioning PMSGs as essential components in modern wind energy systems [8], [9]. A variable-speed PMSG-based (WECS) typically consists of a wind turbine connected directly to a PMSG, accompanied by a full-scale power converter with load supply [10]. Such standalone systems are particularly valuable in remote areas lacking grid access or where connecting to the grid is costly. To ensure reliable energy supply, these systems often include storage battery to store surplus energy from the wind, thus meeting demand during low-wind periods [11].

To maximize energy capture, WECSs often employ a Maximum Power Point Tracking control algorithm. The MPPT's role is crucial as it dynamically adjusts the rotor speed to maintain optimal power generation, even as wind conditions vary. Traditionally, this regulation is achieved using a Proportional-Integral (PI) controller. Although effective, PI controllers face challenges related to parameter tuning and are highly sensitive to

external conditions, particularly in nonlinear or fluctuating environments. These limitations often result in suboptimal performance when managing the complex, variable conditions inherent in wind energy systems [12], [13]. To overcome these challenges, the study introduces an Artificial Neural Network (ANN)-based MPPT controller as an alternative. ANNs offer adaptive and learning capabilities that enhance the system's ability to achieve more efficient tracking of MPP, especially under rapid fluctuations in wind speed. Unlike traditional PI controllers, ANN-based controllers adjust in real-time based on prior data, allowing them to handle nonlinear dynamics more effectively. This adaptability is particularly advantageous for wind systems, where environmental conditions can shift quickly, making static control less effective [14], [15].

Additionally, Backstepping control is applied to the rectifier within the system, enhancing stability and response to variable wind conditions. Backstepping is a nonlinear control technique that improves system stability by ensuring that control actions progressively follow desired states while satisfying stability conditions at each step. It is based on Lyapunov's stability theory, which is critical for guaranteeing that the system remains stable in the face of fluctuations. Backstepping control divides the control design into smaller steps, allowing for more precise and resilient adjustments to the rectifier's output, which directly impacts the overall system's performance [16], [17].

By combining the ANN-based MPPT controller with an Adaptive Backstepping control strategy for the rectifier, this study establishes a comprehensive, robust control framework. This combination not only ensures optimized power extraction but also provides enhanced system flexibility and adaptability in response to vary wind speeds. Such resilience is essential for standalone systems, especially in remote areas where consistent energy output is crucial. The key contributions of this study are outlined as follows:

1.Enhanced MPPT Control: Implementation of an ANN-based MPPT controller that improves response time and adaptability in variable wind speeds.
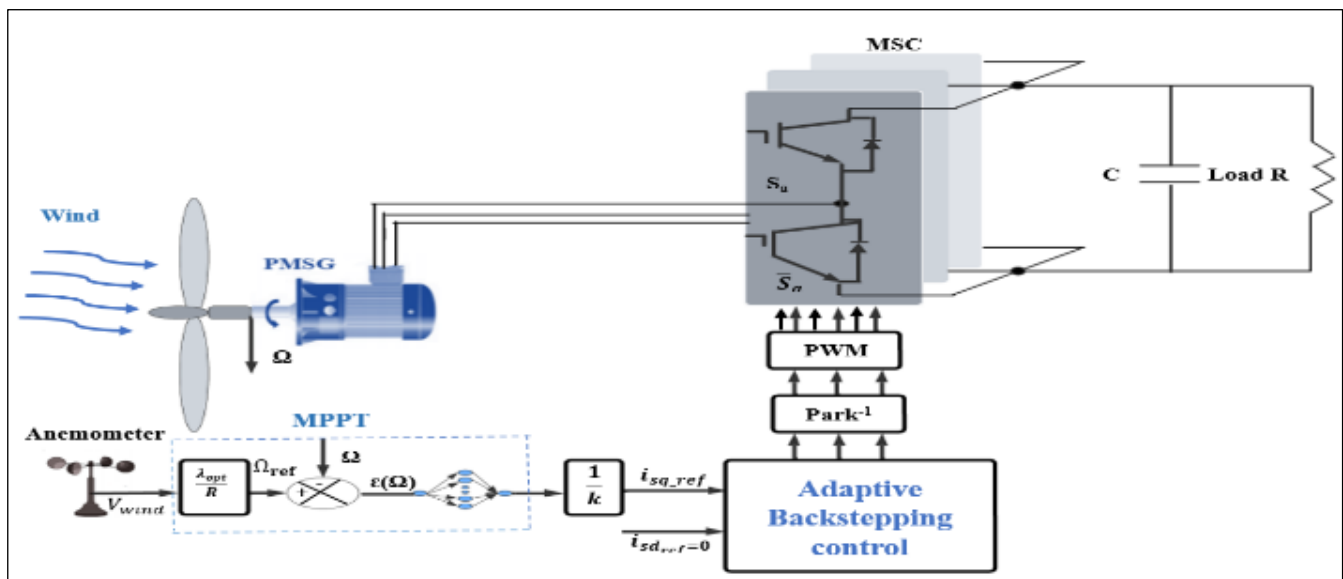

Figure 1: ANN-Backstepping schematic diagram for a PMSG-based wind energy conversion system.
Source: Authors, (2025).

2. **Advanced Backstepping Control:** Utilize a Backstepping control approach founded on Lyapunov's stability theory to optimize the system's overall performance and adaptability to external variations.

3.**Design and Parameterization:** Configuration for a 3kW wind turbine system, providing practical insights for implementing PMSG-based WECS.

4.**Comparative Evaluation:** Analysis of PI and ANN controllers, showing ANN's superiority in handling nonlinear conditions and variable parameters for optimal power extraction.

This article is structured into five sections:

- **Section 1** introduces the study.
- **Section 2** outlines the system configuration, including the aerodynamic model of the wind turbine, the modeling of the permanent magnet synchronous generator, and the MPPT approach.
- **Section 3** delves into the Backstepping control method, providing a detailed analysis of the control laws based on Lyapunov stability theory.

- **Section 4** synthesizes the speed regulator.
- **Section 5** presents the simulation results.

The article concludes with a summary of the main findings and overall conclusions.

II. MODELING AND DESCRIPTION OF THE SYSTEM

II.1 THE SYSTEM CONFIGURATION DESCRIPTION

A WECS typically consists of both electrical and mechanical components. As illustrated in Figure 1, the system analyzed in this study includes a turbine, a (PMSG), a converter (rectifier), and a resistive load R. The turbine converts wind energy into mechanical energy, which is subsequently transformed into electrical energy by the generator. This process involves a machine-side converter (MSC) linked through a DC-link bus. In this study, various control strategies have been explored, including Maximum Power Point Tracking (MPPT) using PI and ANN regulators, as well as Backstepping Control. The subsequent sections detail the mathematical modeling of each component.

II.1.1 WIND TURBINE AERODYNAMIC MODELING

This section aims to model the aerodynamic aspects of the (WECS) with a simplified approach, covering both the wind profile and turbine models. The turbine generates mechanical energy by converting the wind's kinetic energy into usable power [18]. The power available in the wind is described by Equation (1):

$$P_{wind} = \frac{1}{2} \cdot \rho. S. V_{wind}^3 \tag{1}$$

Due to certain physical limitations [19], the wind turbine can only capture a portion of the available wind energy, as represented by the following equation:

$$P_{mec} = C_p(\beta,\lambda). P_{wind} = \frac{1}{2}.\rho. S. C_p(\beta, \lambda). V_{wind}^3 \tag{2}$$

Here, ρ, β, S, and V_{wind} represent the air density, pitch angle, blade area, and wind speed, respectively. The power coefficient C_p, also referred to as the Betz limit, indicates the efficiency of the wind turbine blades in converting the wind's kinetic energy into mechanical energy. This coefficient depends on both the pitch angle (β) and the tip speed ratio (λ), Theoretical studies indicate that the maximum achievable power coefficient is 0.593. However, due to practical limitations—such as blade number, shape, weight, and stiffness—this theoretical maximum cannot be fully achieved. Typically, well-designed turbines achieve power coefficients ranging between 0.4 and 0.5.

The relationship between the aerodynamic power coefficient (C_p) and the tip speed ratio (λ) for varying pitch angles (β) is depicted in Figure 2(a), In this study, the wind turbine achieves maximum power extraction with an efficiency of 0.4535. This optimal performance occurs when the pitch angle (β) is set to zero degrees, and the tip speed ratio (λ) reaches its ideal value of 8.02. The power coefficient (C_p) is expressed by a specific non-linear function as follows:

$$\begin{cases} C_p = 0.5176 \left(\frac{116}{\lambda i} - 0.4\beta - 5 \right) e^{-\frac{21}{\lambda i}} + 0.0068. \lambda \\ \frac{1}{\lambda i} = \frac{1}{\lambda + 0.08. \beta} - \frac{0.035}{1 + \beta^3} \\ \lambda = \frac{R. \Omega}{V_{wind}} \end{cases} \tag{3}$$

The mechanical torque is defined as the ratio of the power supplied to the Permanent Magnet Synchronous Generator (PMSG) to the rotor's mechanical speed. Using Equations (2) and (3), the turbine torque can be calculated using the following formula:

$$T_{mec} = \frac{P_{mec}}{\Omega} = \frac{1}{2}.\frac{\rho. S. R^3. C_p(\beta, \lambda). \Omega^3}{\lambda^3} \tag{4}$$

II.1.2 PERMANENT MAGNET SYNCHRONOUS GENERATOR MODELING

The Permanent Magnet Synchronous Generator (PMSG) plays a crucial role in (WECS) as the primary component responsible for transforming mechanical energy into electrical energy. With power ratings reaching several megawatts, the PMSG is widely preferred due to its significant advantages over traditional synchronous machines [20]. In this study, the dynamic equations describing the operation of the PMSG are formulated in the synchronous rotating reference frame (d-q) as follows:

- Stator volage: $\begin{cases} V_{sd} = R_s. i_{sd} + \frac{d\Psi_d}{dt} - w_r. \Psi_q \\ V_{sq} = R_s. i_{sq} + \frac{d\Psi_q}{dt} - w_r. \Psi_d \end{cases}$ (5)

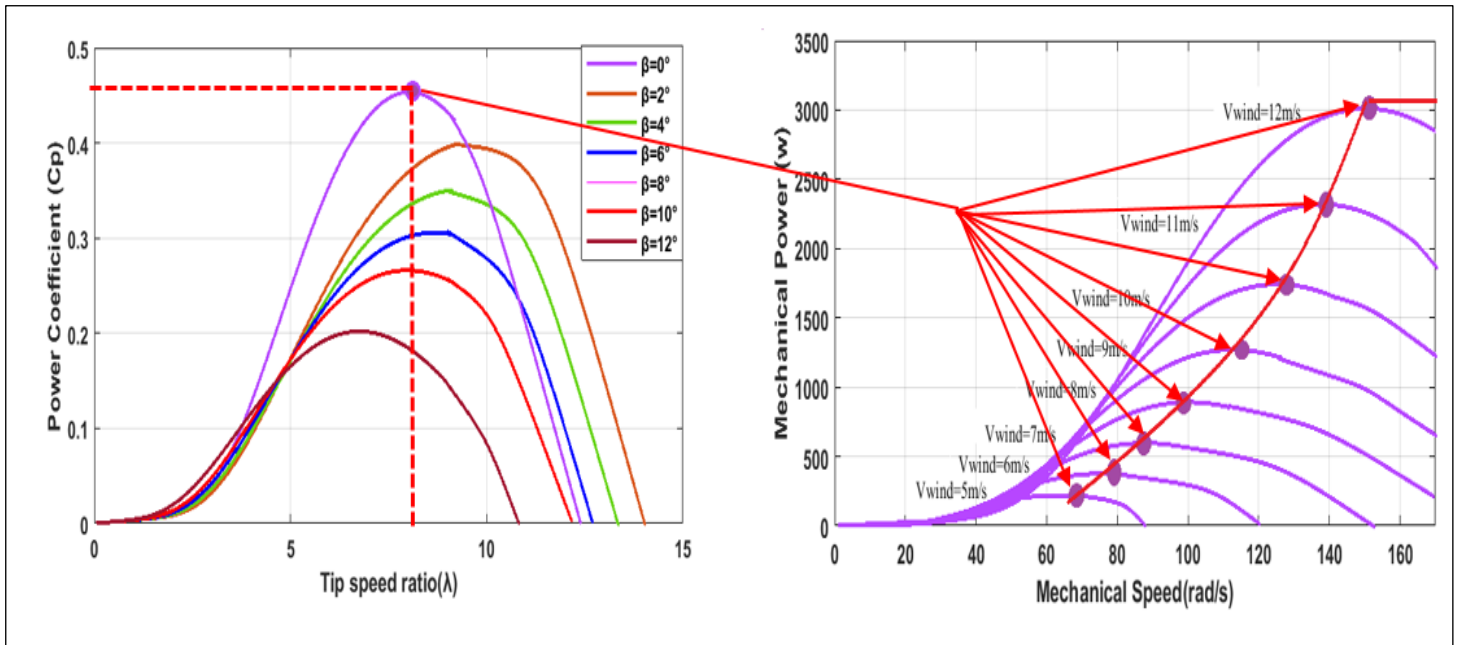- Stator fluxes: $\begin{cases} \Psi_d = L_d. i_{sd} + \Phi_f \\ \Psi_q = L_q. i_{sq} \end{cases}$ (6)

Figure 2: Wind Turbine Characteristics: (a) Cp curve showing variations with pitch angle β, (b) Power and mechanical speed characteristics of the wind turbine at different wind speeds.
Source: Authors, (2025).

This allows writing:

$$\begin{cases} V_{sd} = R_s \cdot i_{sd} + L_d \dfrac{di_{sd}}{dt} - w_r \cdot L_q \cdot i_{sq} \\ V_{sq} = R_s \cdot i_{sq} + L_q \dfrac{di_{sq}}{dt} - w_r \cdot L_d \cdot i_{sd} + w_r \cdot \Phi_f \end{cases} \quad (7)$$

The electromagnetic torque in the Park coordinate system, combined with the mechanical equation, characterizes the system as follows:

$$\begin{cases} T_{tur} - T_{em} = J \cdot \dfrac{d_\Omega}{dt} + f_c \cdot \Omega \\ T_{em} = \dfrac{3}{2} \cdot p \cdot \left[(L_d - L_q) i_{sd} \cdot i_{sq} + \Phi_f \cdot i_{sq} \right] \end{cases} \quad (8)$$

II.1.3 MPPT CONTROL

As shown in Figure 2(b), the maximum energy output varies with wind speed. The rotor speed at maximum energy output is known as the optimal rotor speed (Ω_opt), and MPPT is used to maintain this speed at each wind speed to achieve maximum energy output.

Figure 3 illustrates a block diagram of the wind turbine system incorporating (MPPT) with speed control, adapted from [21].
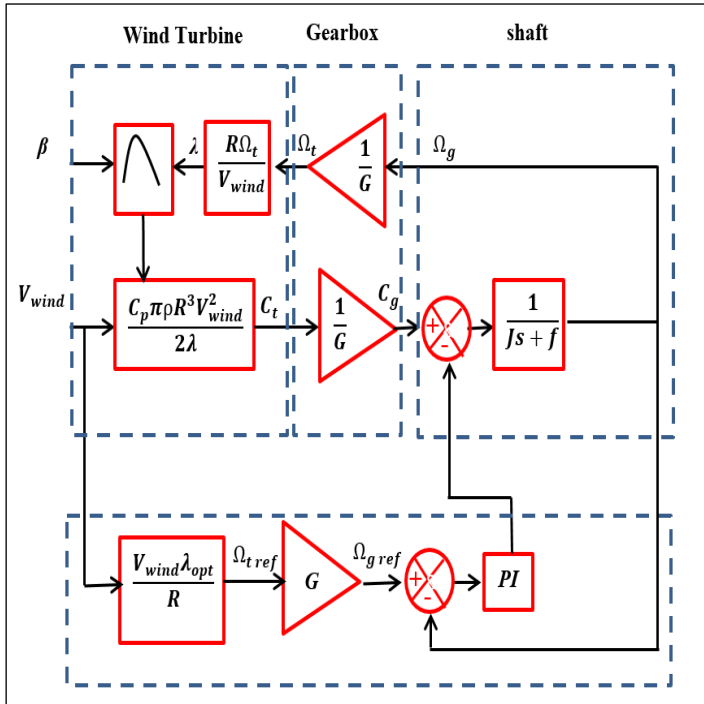

Figure 3: The block diagram of MPPT with speed control.
Source: Authors, (2025).

In a standard (WECS), when the wind speed surpasses the nominal value, a pitch angle control strategy is employed to regulate the turbine's mechanical power output and ensure system safety [22]. However, this study focuses on (MPPT) under the assumption that the wind speed stays below the nominal value. Consequently, the turbine's blade pitch angle is considered fixed during the MPPT operation. In general, the operational range of a (WECS) can be divided into four specific zones based on wind speed, as depicted in Figure 4.
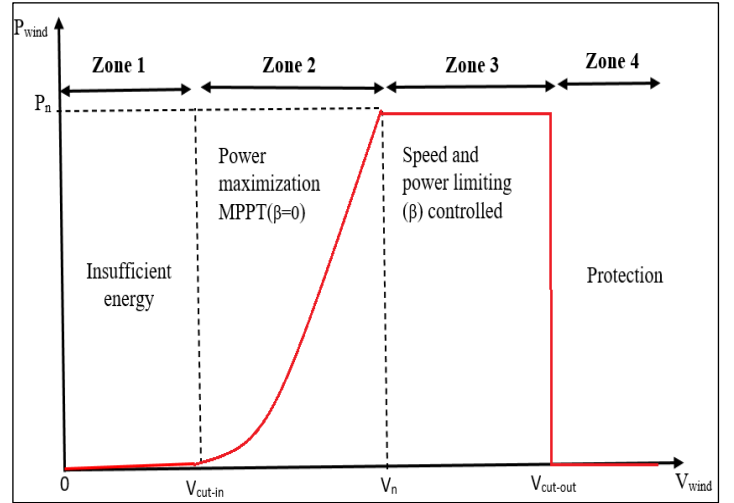

Figure 4: Various operating regions of a wind turbine.
Source: Authors, (2025).

III. IMPLEMENTATION OF ADAPTIVE BACKSTEPPING CONTROL IN PMSG-BASED WIND ENERGY SYSTEMS

III.1 MACHINE SIDE CONTROL

Backstepping control is a structured approach used to design controllers for nonlinear systems, making it suitable for a diverse range of applications [23]. Its concept is based on breaking down a complex system into a series of interconnected first-order subsystems, where a virtual control law is first developed for a small subsystem and then extended iteratively to the entire system. A Lyapunov function is constructed during this process to ensure system stability [24]. Backstepping is categorized into two techniques: The non-adaptive backstepping algorithm assumes that all system parameters, including those related to the PMSG, are fully known and remain constant. However, this assumption is often unrealistic in practical applications, as parameters can vary due to factors such as temperature changes, magnetic saturation effects, and variations in load torque. Consequently, it is essential to consider the nonlinearities and uncertainties introduced by these unknown parameters when designing the controller. To improve the system's robustness against parameter variations and measurement noise, estimators, often called observers, are commonly employed. The adaptive backstepping control algorithm leverages these estimations to achieve more precise approximations of the actual system parameters, including those related to the PMSG [25]. The method is fundamentally used to regulate system parameters, such as electromagnetic torque, within a vector control framework by controlling stator voltages. Stator current components (i_{sd} and i_{sq}) in the rotating frame are managed to achieve torque control through i_{sq} and flux control through i_{sd}. Reference voltages applied to the machine's side converter determine the control signals for rectifier arms, ensuring precise regulation of the system [26]. Based on Equations (7) and (8), the system model is clearly outlined as follows:

$$\begin{cases} \dfrac{di_{sd}}{dt} = \dfrac{1}{L_d} \left(-R_s \cdot i_{sd} + p \cdot \Omega \cdot L_q \cdot i_{sq} + V_{sd} \right) \\ \dfrac{di_{sq}}{dt} = \dfrac{1}{L_d} \left(-R_s \cdot i_{sq} - p \cdot \Omega \cdot L_d \cdot i_{sd} - p \cdot \Omega \cdot \Phi_f + V_{sq} \right) \\ \dfrac{d\Omega}{dt} = \dfrac{1}{J} \left(T_{tur} - T_{em} - f_c \cdot \Omega \right) \end{cases} \quad (9)$$

STEP 1: MECHANICAL SPEED CONTROLLER DESIGN:

The speed tracking error can be expressed using the following equation:

$$e_\Omega = \Omega_{ref} - \Omega \qquad (10)$$

The derivative is expressed as:

$$\dot{e}_\Omega = \dot{\Omega}_{ref} - \dot{\Omega}$$
$$= \dot{\Omega}_{ref} - \frac{1}{J}\left[T_{tur} - \frac{3p}{2}\left((L_d - L_q)i_{sd}.i_{sq} + i_{sq}.\Phi_f\right) - f_c.\Omega\right] \quad (11)$$

The initial step ensures the tracking of the reference speed, thereby eliminating the speed error. To achieve this, Lyapunov's function is utilized:

$$V_1 = \frac{1}{2}e_\Omega^2 \qquad (12)$$

The derivative of Lyapunov's function is expressed as follows:

$$\dot{V}_1 = e_\Omega.\dot{e}_\Omega$$
$$= -k_\Omega e_\Omega^2 + \frac{e_\Omega}{J}\left(-T_{tur} + f_c\Omega + k_\Omega.J.e_\Omega + \frac{3p}{2}.i_{sq}.\Phi_f\right) + \frac{3}{2J}p(L_d - L_q)i_{sd}.i_{sq}.e_\Omega \quad (13)$$

To guarantee the stability of the first subsystem, it is essential to select $\dot{V}_1$ as negative. This selection leads to the appropriate determination of the stator currents i_{sd} and i_{sq}.

$$\begin{cases} i_{sd\_ref} = 0 \\ i_{sq\_ref} = \frac{2}{3.p.\Phi_f}(T_{tur} - f_c.\Omega - k_\Omega.J.e_\Omega) \end{cases} \qquad (14)$$

The virtual references i_{sd_ref} and i_{sq_ref} are defined for the second step. Substituting i_{sd_ref}, i_{sq_ref} and $\dot{\Omega}_{ref} = 0$ into Equation (13) yields:

$$\dot{V}_1 = -k_\Omega.e_\Omega^2 \leq 0 \qquad (15)$$

The system represented by Equation (15) will remain stable if k_Ω is chosen as a positive constant.

STEP 2: DESIGNING THE STATOR CURRENT CONTROLLER:

In the second step of this algorithm, the control voltages V_{sd_ref} and V_{sq_ref}, which are determined based on the system's virtual inputs, specifically the stator currents (i_{sd}, i_{sq}). The errors in the stator currents are defined by the following equations:

$$e_d = i_{sd\_ref} - i_{sd} \qquad (16)$$

$$e_q = i_{sq\_ref} - i_{sq} \qquad (17)$$

Using Equations (16) and (17), the dynamic behavior of the current errors e_d and e_q can be expressed as:

$$\dot{e}_d = \dot{i}_{sd_{ref}} - \dot{i}_{sd} = 0 - \dot{i}_{sd}$$
$$= \frac{1}{L_d}\left(R_s.i_{sd} - p.\Omega.L_q.i_{sq} - V_{sd}\right) \qquad (18)$$

$$\dot{e}_q = \dot{i}_{sq_{ref}} - \dot{i}_{sq} = \frac{2}{3.p.\Phi_f}(-f_c\Omega - k_\Omega.J.\dot{e}_\Omega)$$
$$+ \frac{1}{L_q}\left(R_s.i_{sq} + p.L_d.\Omega.i_{sd} + p.\Omega.\Phi_f - V_{sq}\right) \qquad (19)$$

With:

$$\dot{e}_\Omega = \frac{1}{J}\left[-k_\Omega.J.e_\Omega - \frac{3p}{2}\Phi_f.e_q - \frac{3p}{2}.(L_d - L_q)i_{sd}.i_{sq}\right] \qquad (20)$$

The expression for $\dot{e}_q$ is then given as:

$$\dot{e}_q = \frac{2}{3.p.\Phi_f} \times$$
$$\left((k_\Omega.J - f_c)\left[T_{tur} - f_c\Omega - \frac{3p}{2}.(L_d - L_q)i_{sd}.+i_{sq}.\Phi_f\right]\right)$$
$$+ \frac{1}{L_q}\left(R_s.i_{sq} + p.\Omega.L_d.i_{sd} + p.\Omega.\Phi_f - V_{sq}\right) \qquad (21)$$

As the system grows more complex, incorporating three state variables, it becomes essential to choose a second Lyapunov function to calculate the stator voltage references. This function considers both the rotational speed error and the stator current errors:

$$V_2 = \frac{1}{2}\left(e_\Omega^2 + e_d^2 + e_q^2\right) \qquad (22)$$

By applying Equations (18), (20), and (21), the derivative of the second Lyapunov function is obtained as:

$$\dot{V}_2 = \left(e_\Omega.\dot{e}_\Omega + e_d.\dot{e}_d + e_q\dot{e}_q\right) \qquad (23)$$

$$\dot{V}_2 = -k_\Omega.e_\Omega^2 - k_d.e_d^2 - k_q.e_q^2$$
$$+ \frac{e_\Omega}{J}\left(-\frac{3p}{2}.\Phi_f.e_q - \frac{3p}{2}(L_d - L_q)i_{sd}.i_{sq}\right)$$
$$+ \frac{e_d}{L_d}\left(R_s.i_{sd} - p\Omega.L_q.i_{sq} - V_{sd} + k_d.L_d.e_d\right)$$
$$+ \frac{e_q}{L_q}\left[\frac{2.L_q}{3.p.J.\Phi_f}\left((k_\Omega.J - f_c)\left[T_{tur} - f_c.\Omega - \frac{3.p}{2}.(L_d - L_q)i_{sd}.i_{sq} + i_{sq}.\Phi_f\right]\right) + R_s.i_{sq} + p.\Omega.L_d.i_{sq} + p.\Omega.\Phi_f - V_{sq} + k_q.L_q.e_q\right] \qquad (24)$$

Based on Lyapunov's theorem, the stability of the subsystem is guaranteed when the derivative of V_1 to be negative. Therefore, k_d and k_q are assigned positive values, and the following voltages are utilized as reference voltages:

$$\begin{cases} V_{sd_{ref}} = R_s.i_{sd} - p.\Omega.L_q.i_{sq} \\ \quad + k_q.L_q.e_q - \frac{3.p}{2.J}.L_d(L_d - L_q)i_{sd}.e_\Omega \\ V_{sq_{ref}} = \frac{2.L_q}{3.p.J.\Phi_f} \\ \left((k_\Omega.J - f_c)\left[T_{tur} - f_c.\Omega - \frac{3.p}{2}.(L_d - L_q)i_{sd}.i_{sq} + i_{sq}.\Phi_f\right]\right) \\ \quad + R_s.i_{sq} + p.\Omega.L_d.i_{sd} + k_q.L_q.e_q - \frac{3}{2.J}p.i_{sq}.\Phi_f.e_\Omega \end{cases} \qquad (25)$$

IV. SYNTHESIS OF THE SPEED REGULATOR

IV.1 PROPORTIONAL-INTEGRAL (PI)

As shown in Figure 2, the MPPT control strategy has been integrated into the traditional Backstepping control approach. This method aims to enhance the performance of WECS by ensuring optimal wind power extraction at both low and high wind speeds. Moreover, it guarantees that the generator operates within a safe speed range to protect the system [27]. As previously discussed in

this study, the wind turbine achieves its peak power output when the power coefficient (Cp) equals 0.4535. To maintain this level of efficiency, the turbine's rotational speed is continuously regulated through the use of a Proportional-Integral (PI) controller, as illustrated in Figure 5.
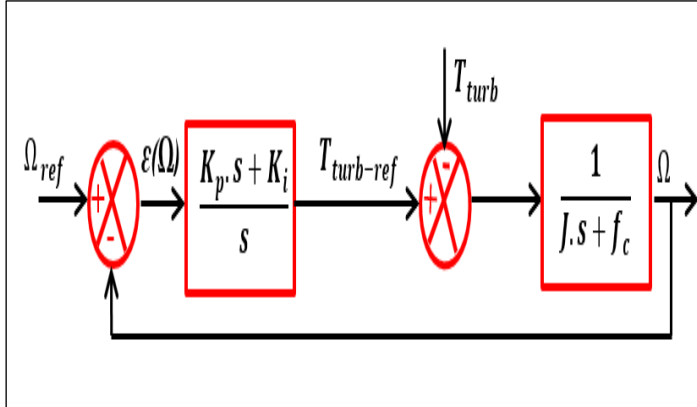

Figure 5: Closed-loop system with the PI.
Source: Authors, (2025).

The design of the PI controller is as follows:

$$PI = \left(\frac{k_p s + k_i}{s}\right) \qquad (26)$$

IV.2 ARTIFICIAL NEURAL NETWORK (ANN)

To improve the system's performance across various wind conditions, the PI controller was substituted with a regulator based on an Artificial Neural Network (ANN).

An Artificial Neural Network (ANN) is a computational model inspired by the architecture and behavior of biological nervous systems. It imitates human cognitive capabilities, enabling machines to interpret and process information in a way similar to human thought patterns.

ANNs consist of interconnected neurons that are organized into layers: input, hidden, and output layers, where the data is received, processed, and transmitted [28]. These neurons work in parallel and are connected by adjustable numerical weights that are fine-tuned during the learning process [29]. The theoretical model of a basic neuron is represented by the following equation:

$$y_i^{ANN} = f(\sum_i^n w_i x_i + b) \qquad (27)$$

The variables n, y_i^{ANN}, f, $x\{x_i, i=1,2,\ldots,n\}, w_i$ and b represent the number of neural network inputs, the output vector of the network, the activation function, the neural network input vector, the weight matrix, and the bias, respectively. Typically, the bias input is set to either +1 or −1, and the weight matrix is adjusted using the backpropagation method.

The neuron serves as the fundamental building block of artificial neural networks, encompassing summation and activation functions [30], as shown in figure 6.
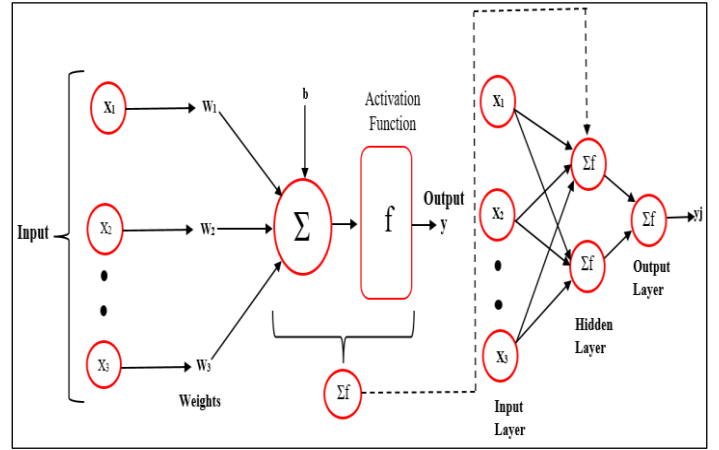

Figure 6: Structure of artificial neural network (ANN) model.
Source: Authors, (2025).

IV.2.1 DESIGNING THE ANN MODEL

The initial phase in constructing the Artificial Neural Network (ANN) requires gathering the necessary datasets. In this research, the datasets were derived from simulation outcomes, focusing on input and output values of the system's speed regulator (PI). Wind speed data was also incorporated during model development to ensure a comprehensive representation. The acquired data was randomly divided into three categories for training, validation, and testing purposes:

- **70%** of the data was allocated for training.
- **15%** was used for validation.
- **15%** was reserved for testing.

In the next phase, the ANN controller was implemented using MATLAB's user-friendly graphical interface, specifically the "nntool" feature available in MATLAB R2021a. It should be emphasized that the efficiency of the ANN controller is affected by various elements, including the number of neurons in the hidden layer, the type of activation function used, and the training algorithm selected [31].

IV.2.2 PERFORMANCE EVALUATION

The evaluation of the trained ANN models was conducted using the Mean Squared Error (MSE), which measures the average squared difference between the predicted outputs of the network and the target values. A reduction in MSE during simulations indicates an ANN controller with improved accuracy, signifying a better alignment between the predictions of the model and the expected outputs. During training, the weight adjustments were performed iteratively using the Levenberg-Marquardt backpropagation algorithm. This iterative training process continued over multiple cycles until the error was reduced to an acceptable level. If the error failed to converge satisfactorily, modifications were applied to the ANN structure, such as increasing or decreasing the number of hidden neurons or changing the configuration of hidden layers [32].

As shown in Figure 7(a) and (b), the ANN-based speed controller achieved exceptional performance, with a minimal MSE of 0.00217 and 6.3528e-5, demonstrating a high degree of alignment between the output and target values. The optimal configurations of the proposed ANN models are summarized in Table 1.

Table 1: ANN architecture and training parameters.

| ANN Parameter	Speed Controller (wind speed under Step Profil)	Speed Controller(wind speed under random Profil)
Neuron network architecture	Multi-Layer Perceptron Feedforward	Multi-Layer Perceptron Feedforward
Inputs/ Outputs Data	Ɛ(Ω)/Tem-ref	Ɛ(Ω)/Tem-ref
Number of neurons: Input layer Hidden layer 1 Hidden layer 2 Hidden layer 3 Output layer	1 25 10 - 1	1 5 10 5 1
Hidden activation	Tansig	Tansig
Output activation	Purline	Purline
Training function (Algorithm)	Trainlm (Levenberg-Marquardt algorithm)	Trainlm (Levenberg-Marquardt algorithm)
Number of epochs	400	548
Learning rate	0.1	0.1
Training goal	0	0
Performance function	0.0021704	6.3528e-5

Source: Authors, (2025).
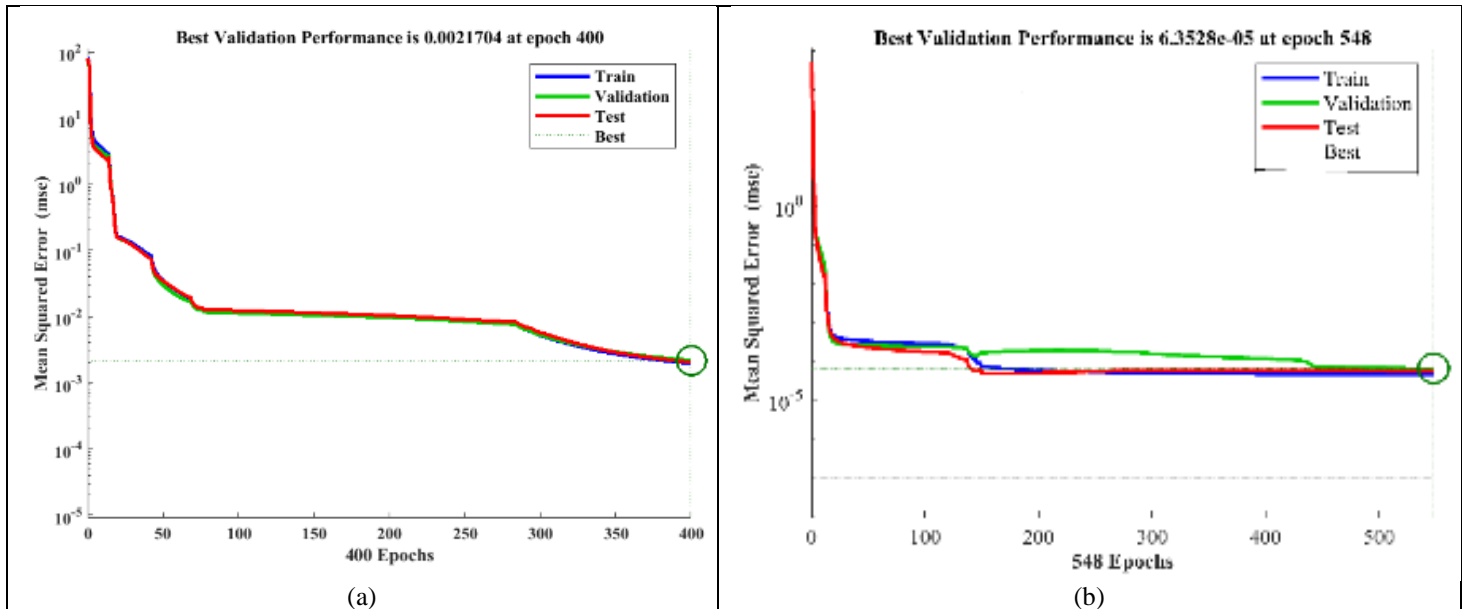
Figure 7: (a)Training performance based on MSE (Step Profil), (b) Training performance based on MSE (Random Profil)
Source: Authors, (2025).

V. RESULTS AND DISCUSSIONS

To evaluate the effectiveness of the proposed control scheme, a 3 kW PMSG-based (WECS) was simulated using MATLAB/Simulink. The simulation parameters for the power synchronous generator and turbine under varying wind conditions are detailed in Tables A.1 and A.2 in Appendix A. This study conducted two tests to compare the effectiveness, performance, and robustness of the proposed ANN-Backstepping control method with the PI-Backstepping approach. Additionally, the tests evaluated the impact of these control strategies on the system's dynamic behavior. In the first test, the wind speed (WS) profile was subjected to step changes, including both increases and decreases. The second test used a randomly varying WS profile to evaluate system response.
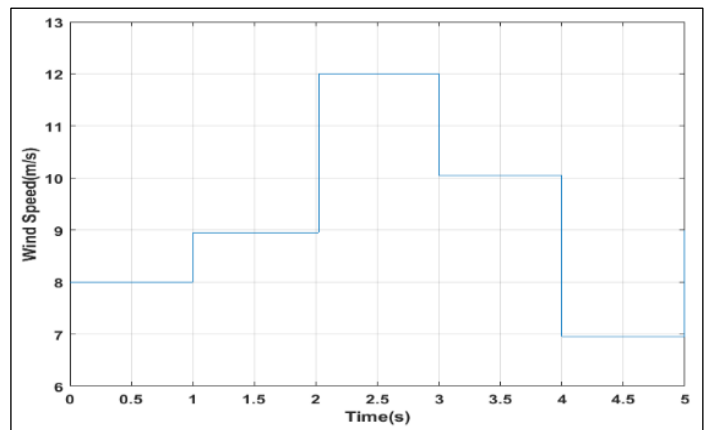

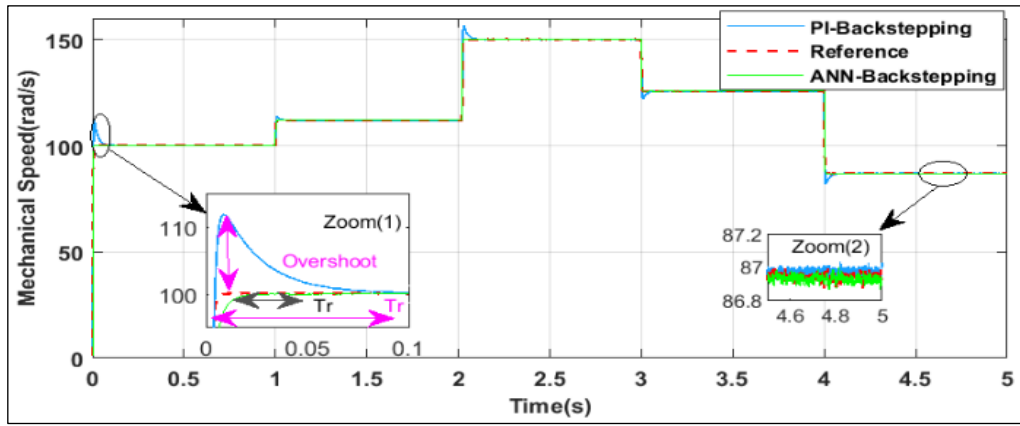Figure 8: Wind speed profile
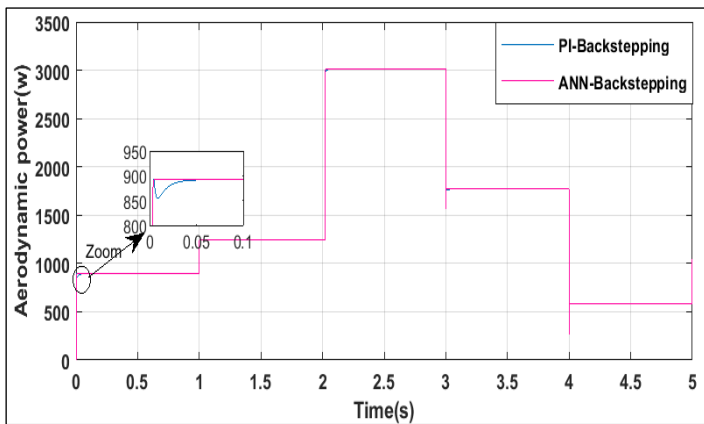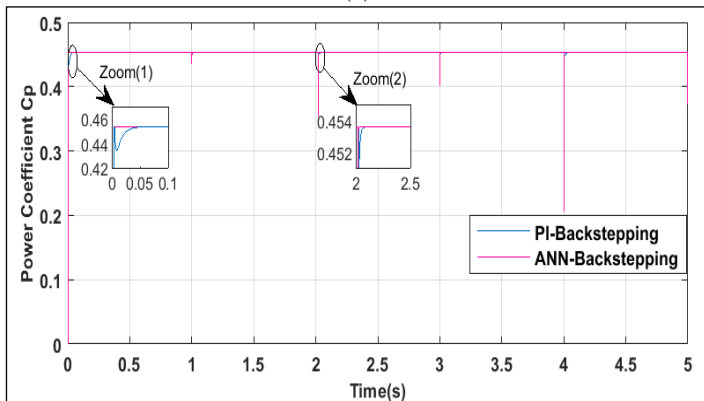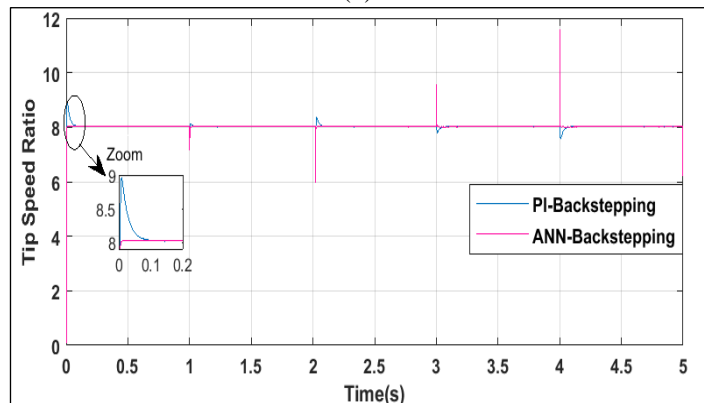Source: Authors, (2025).

Figure 9: Mechanical Speed of the PMSG
Source: Authors, (2025).

(a)
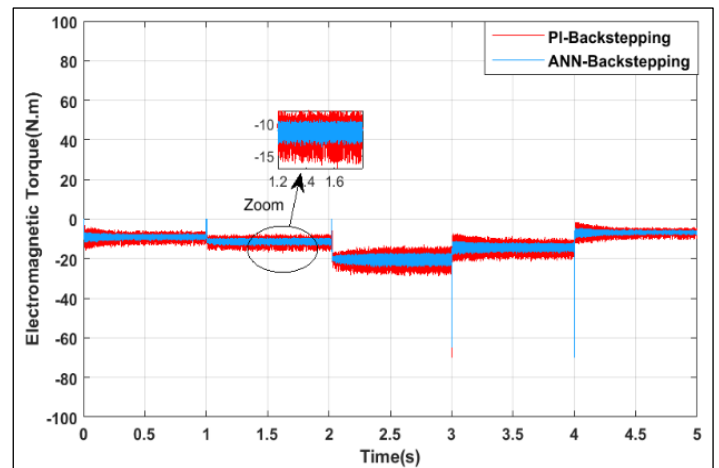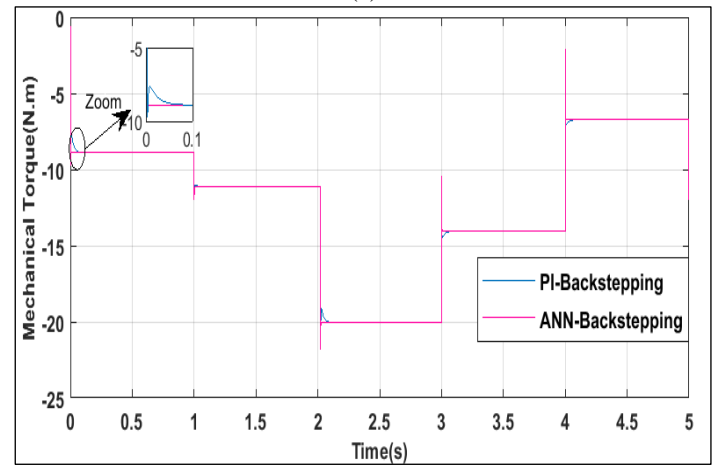

(b)

(c)

Figure 10: (a) Aerodynamic Power, (b) Power Coefficient Cp
and (c) Tip Speed Ratio λ
Source: Authors, (2025).

(a)

(b)

Figure 11: (a) Electromagnetic Torque, (b) Mechanical Torque
Source: Authors, (2025).

V.1. STEP PROFILE

As illustrated in Figure 8, the wind speed profile experiences step changes within a 5-second time span. Figures 9 and 10(a) illustrate the mechanical speed (Ω) and aerodynamic power of the system when employing the PI-Backstepping and ANN-Backstepping control strategies, respectively. It is evident that both the mechanical speed and aerodynamic power closely follow their reference values, mirroring the shape of the wind speed profile. However, as highlighted in Zoom (1) of Figure 9, the mechanical speed controlled by the PI-Backstepping approach

exhibits a significant overshoot of 12%, whereas the ANN-Backstepping control eliminates this overshoot entirely. A similar observation can be made for the aerodynamic power in the zoomed-in view of Figure 10(a). Additionally, ANN-Backstepping offers a shorter settling time and reduced tracking error, as demonstrated in Zoom (2) of Figure 9, further validating the effectiveness of the proposed control strategy. Furthermore, Figures 10(a) and 10(b) depict the power coefficient (Cp) and the tip speed ratio (λ), which maintain a close alignment with their reference values under the ANN-Backstepping control. This approach achieves minimal tracking errors and no overshoot, even during wind speed fluctuations, outperforming the PI-Backstepping method. These findings confirm that the system operates near its optimal rotational speed and demonstrate the superior efficiency of the proposed ANN-Backstepping control in terms of settling time, overshoot, and precision compared to the PI-Backstepping control.

Backstepping achieves better control with reduced fluctuations, highlighting its superior disturbance handling. Both strategies stabilize after disturbances, but ANN-Backstepping shows better torque regulation throughout. Figure 11(b) demonstrate Mecanichal torque. Both strategies track these step changes, but ANN-Backstepping (pink) demonstrates a slightly faster and smoother response compared to PI-Backstepping (blue). The zoomed-in section (0 to 0.1s) highlights the reaction to an abrupt torque

change. ANN-Backstepping shows reduced overshoot and better tracking precision.

As depicted in Figure 12, the currents of a (PMSG), illustrating the behavior of three-phase currents, and under specific operating conditions. The currents oscillate sinusoidally, maintaining a balanced three-phase system. This indicates proper functioning of the PMSG, with the phases remaining symmetric under normal conditions. Zoomed Section (2.4–2.42s) this magnified view reveals the detailed sinusoidal nature of the currents. After the transient period, the current waveforms gradually return to their steady-state sinusoidal pattern, demonstrating the system's ability to recover and reestablish balance.
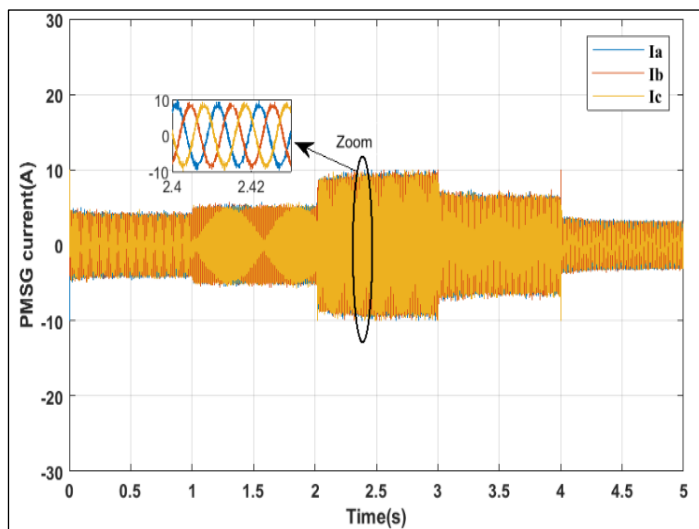

Figure 12: PMSG current
Source: Authors, (2025).

Figure 11(a) demonstrate electromagnetic torque . Both PI-Backstepping (red) and ANN-Backstepping (blue) are compared, showing that ANN-Backstepping exhibits smoother performance with fewer oscillations during transient conditions. The zoomed section between 1.2s and 1.6s emphasizes that ANN-
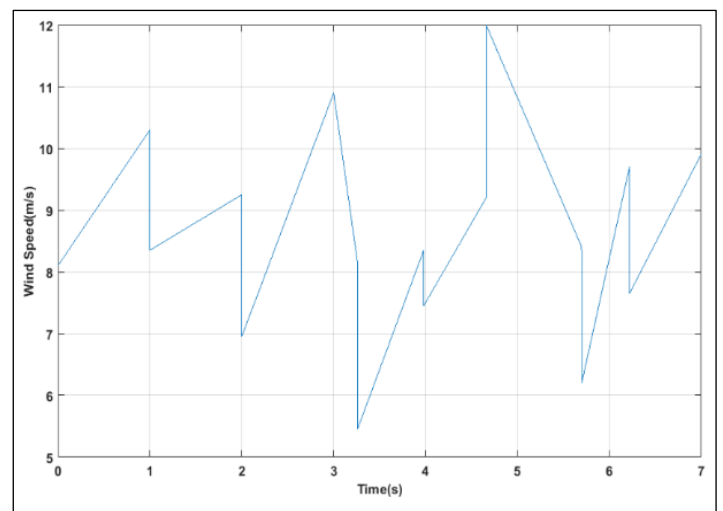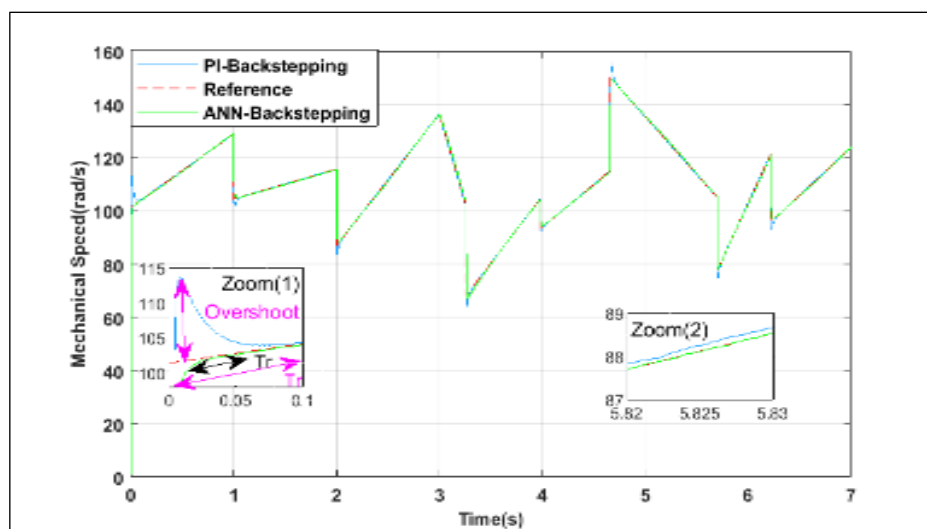

Figure 13: Wind speed profile
Source: Authors, (2024).

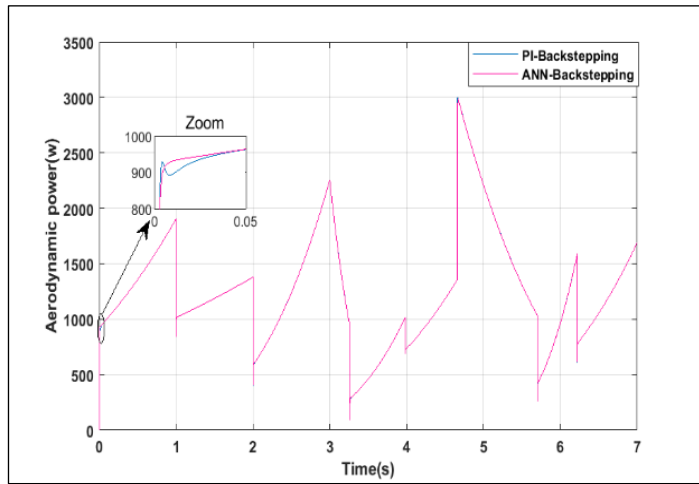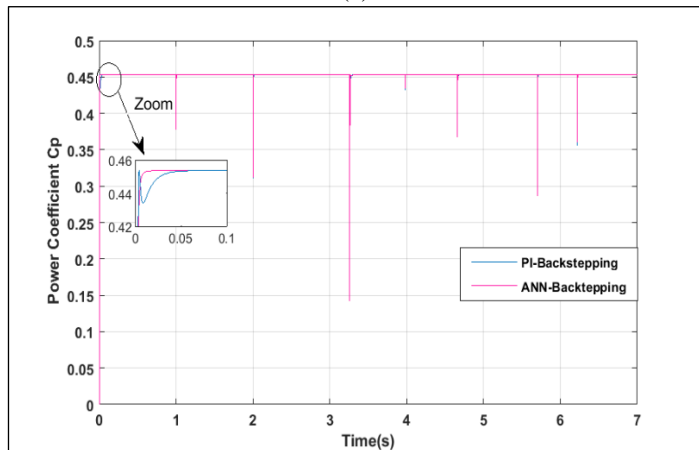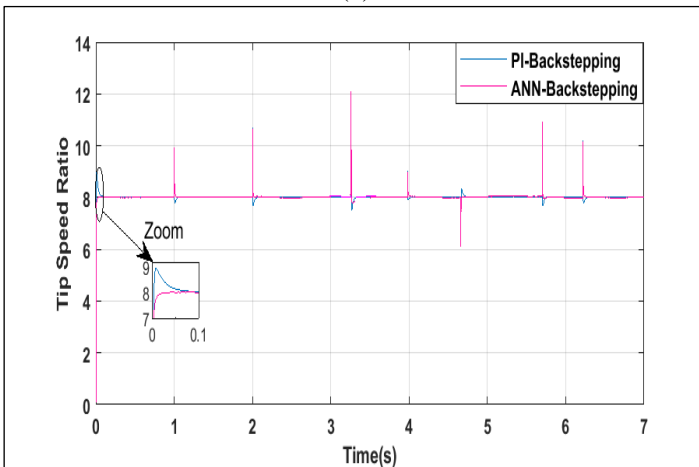

Figure 14: Mechanical Speed of the PMSG.
Source: Authors, (2025).

(a)

(b)

(c)

Figure 15: (a) Aerodynamic Power, (b) Power Coefficient Cp and (c) Tip Speed Ratio λ
Source: Authors, (2025).

V.2. RANDOM PROFILE

This section examines the stability of the evaluated control system under conditions of random wind speed variations, as illustrated in Figure 13.These variations highlight the challenges faced by control systems in maintaining stable performance in fluctuating wind Scenarios. In the Figure 14 (mechanical speed) offers a comparison between two control techniques: PI-Backstepping and ANN-Backstepping, with a reference value. Key observations include:

Zoom 1 (Overshoot and Settling Time): ANN-Backstepping shows reduced overshoot and quicker settling time, indicating superior dynamic response.
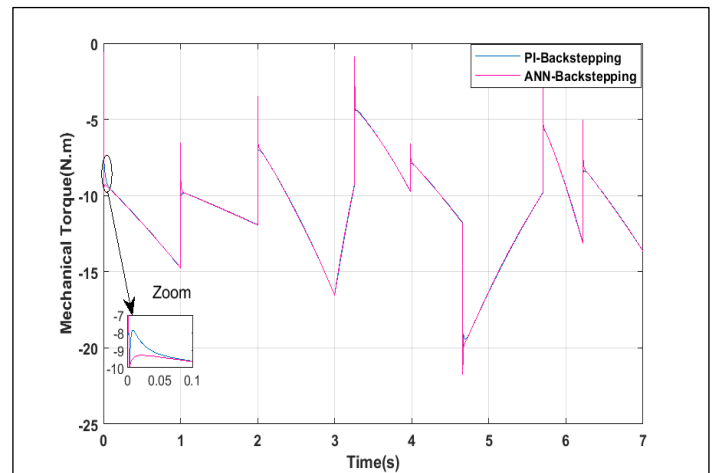

Figure 16: Mechanical Torque.
Source: Authors, (2025).

Zoom 2 (Steady-State Stability): The ANN-Backstepping method demonstrates closer adherence to the reference signal during steady-state operation, confirming its improved accuracy.

As shown in Figure 15(a), evaluates the aerodynamic power output under the two control strategies. ANN-Backstepping displays a more consistent response across time, with smoother transitions and better tracking of power fluctuations compared to PI-Backstepping. The inset zoom highlights the rapid stabilization of aerodynamic power during initial transient conditions, where ANN-Backstepping shows an advantage in handling disturbances. Figures 15(b) and (c) illustrate the successful achievement of MPPT, as the Cp and λ values are maintained at their optimal and most desirable levels, respectively. The proposed ANN-Backstepping method for MPPT guarantees quick stabilization of the optimal power coefficient while consistently preserving the ideal λ value. Figure 16 demonstrate Mecanichal torque. This plot showcases the mechanical torque dynamics of the system under both control methods. The following is evident:

ANN-Backstepping provides smoother torque transitions, which can reduce mechanical stress and enhance system longevity.

In the zoomed-in view, ANN-Backstepping again achieves quicker stabilization and smaller torque deviations compared to PI-Backstepping, emphasizing its improved disturbance rejection capabilities.

VI. CONCLUSIONS

This study aimed to enhance the performance of wind energy systems by focusing on a wind turbine coupled with a (PMSG), rectifier converter, and load. The research evaluated and validated the efficiency of control strategies, particularly Backstepping control for PMSG and (MPPT). Initially, a PI regulator was employed for MPPT, which was later replaced with an (ANN) for improved performance.

The key scientific contributions of this work are as follows:

✓ The integration of Backstepping control with PMSG demonstrated superior system stability and robustness.

- ✓ The replacement of the traditional PI regulator with ANN for MPPT significantly improved power tracking accuracy and dynamic response.

- ✓ Enhanced dynamic aerodynamic power quality and faster response times were achieved.

- ✓ The ANN-based MPPT control reduced tracking errors and ensured optimal performance under varying wind profiles.

The simulation results confirmed that combining Backstepping control with ANN-based MPPT offers a robust and efficient solution for wind energy systems. This approach not only ensures consistent power output but also optimizes the overall energy harvesting efficiency, making it a valuable contribution to renewable energy research. Future work will focus on analyzing the dynamic performance of a PMSG-based wind energy conversion system under varying load conditions.

APPENDIX A

Table A.1: parameters for the power synchronous generator.

Parameter	Value
Rated generator power (Pn)	3kW
Stator Inductance (L_s)	0.0076 H
Pole pairs (p)	4
Permanent magnet flux Φ_f	0.4 Wb
Coefficient of friction(f)	0.00016900 kg.m^2.s^{-1}
Moment d'inrtie (J)	0.0032 kg.m^2
Stator Resistance (R_s)	2.3 Ω

Source: Authors, (2025).

Table A.2: Parameters of the turbine.

Parameter	Value
Radius of the turbine blade (R)	1.41m
The air density (ρ)	1.23 kg/m^3
Tip-speed ratio (λ)	8.02
Power Coefficient (Cp)	0.4535

Source: Authors, (2025).

VII. AUTHOR'S CONTRIBUTION

Conceptualization: Wassila Hattab, Abdelhamid Benakcha, Seddik Tabet, Amira Slimani.
Methodology: Wassila Hattab, Abdelhamid Benakcha, Seddik Tabet, Amira Slimani.
Investigation: Wassila Hattab, Abdelhamid Benakcha, Seddik Tabet, Amira Slimani.
Discussion of results: Wassila Hattab, Abdelhamid Benakcha, Seddik Tabet, Amira Slimani.
Writing – Original Draft: Wassila Hattab, Abdelhamid Benakcha, Seddik Tabet, Amira Slimani.

Writing – Review and Editing: Wassila Hattab, Abdelhamid Benakcha, Seddik Tabet, Amira Slimani.
Supervision: Wassila Hattab, Abdelhamid Benakcha, Seddik Tabet, Amira Slimani.
Approval of the final text: Wassila Hattab, Abdelhamid Benakcha, Seddik Tabet, Amira Slimani.

VIII. REFERENCES

[1] M. W. Ayub, A. Hamza, G. A. Aggidis, and X. Ma, "A review of power co-generation technologies from hybrid offshore wind and wave energy," Energies, vol. 16, no. 550, 2023. [Online]. Available: https://doi.org/10.3390/en16010550

[2] F. Bakhtiari and J. Nazarzadeh, "Optimal estimation and tracking control for variable-speed wind turbine with PMSG (in)," J. Modern Power Syst. Clean Energy, vol. 8, no. 1, pp. 159–167, 2020. [Online]. Available: https://doi.org/10.35833/MPCE.2018.000365

[3] A. Sajadi, L. Strezoski, A. Khodaei, K. Loparo, M. Fotuhi-Firuzabad, R. Preece, M. Yue, F. Ding, V. Levi, P. Arboleya, et al., "Guest editorial: Special issue on recent advancements in electric power system planning with high-penetration of renewable energy resources and dynamic loads," Int. J. Electr. Power Energy Syst., vol. 129, pp. 106597, 2021. [Online]. Available: https://doi.org/10.1016/j.ijepes.2021.106597

[4] D. Fu, L. Kong, L. Gong, A. Wang, H. Jia, and N. Zhao, "Wind turbine load optimization control strategy based on LIDAR feed-forward control for primary frequency modulation process with pitch angle reservation," Energies, vol. 16, no. 510, 2023. [Online]. Available: https://doi.org/10.3390/en16010510

[5] Y. El Mourabit, A. Derouich, A. ElGhzizal, N. El Ouanjli, and O. Zamzoum, "Nonlinear backstepping control of variable speed wind turbine based on permanent magnet synchronous generator," in Proc. Int. Conf. Wireless Technol., Embedded Intell. Syst. (WITS), Fez, Morocco, 2019, pp. 1–7. [CrossRef]

[6] A. Ullah, M. Ahmed, S. A. Raza, and S. Ali, "A threshold approach to sustainable development: Nonlinear relationship between renewable energy consumption, natural resource rent, and ecological footprint (Oct.)," J. Environ. Manag., vol. 295, pp. 113073, 2021. [Online]. Available: https://doi.org/10.1016/j.jenvman.2021.113073

[7] F. Huerta, R. Tello, and M. Prodanovic, "Real-time power hardware-in-the-loop implementation of variable-speed wind turbines," IEEE Trans. Ind. Electron., vol. 64, no. 3, pp. 1893–1904, Mar. 2017. [Online]. Available: https://doi.org/10.1109/TIE.2016.2623253

[8] D. Karboua, Y. Chouiha, B. O. Douara, I. F. Bouguenna, S. Benkaihoul, and B. Toual, "Advanced Dual-Loop Control Architecture for Superior PMSM Performance Utilizing Finite-Control-Set Model Predictive Control and Exponential Reaching Law Sliding Mode Control," *Journal of Engineering and Technology for Industrial Applications (ITEGAM-JETIA)*, vol. 10, no. 49, pp. 71-79, Sep./Oct. 2024. [Online]. Available: https://doi.org/ 10.5935/jetia.v10i49.1221

[9] M. E. Zarei, D. Ramírez, M. Prodanovic, and G. M. Arana, "Model predictive control for PMSM-based wind turbines with over modulation and adjustable dynamic response time," IEEE Trans. Ind. Electron., vol. 69, no. 2, pp. 1573–1585, 2021. [Online]. Available: https://doi.org/10.1109/TIE.2020.2973206

[10] J. Wang, D. Bo, X. Ma, Y. Zhang, Z. Li, and Q. Miao, "Adaptive back-stepping control for a permanent magnet synchronous generator wind energy conversion system," Int. J. Hydrogen Energy, vol. 44, no. 19, pp. 3240–3249, 2019. [Online]. Available: https://doi.org/10.1016/j.ijhydene.2018.12.133

[11] S. Sahu, G. Panda, and S. P. Yadav, "Dynamic modelling and control of PMSG based stand-alone wind energy conversion system," in Proc. Recent Adv. Eng., Technol. Comput. Sci. (RAETCS), Nat. Inst. Technol. Meghalaya, India, 2018.

[12] J. Pande, D. Nasikkar, K. Kotecha, and V. Varadarajan, "A review of maximum power point tracking algorithms for wind energy conversion systems (Oct.)," J. Mar. Sci. Eng., vol. 9, no. 1187, 2021. [Online]. Available: https://doi.org/10.3390/jmse9111187.

[13] A. A. Iqbal and N. Akhtar, "A comprehensive review of MPPT techniques for wind energy systems," Renewable and Sustainable Energy Reviews, vol. 69, pp. 1246–1260, 2017. [Online]. Available: https://doi.org/10.1016/j.rser.2016.11.243

[14] J. C. Guerrero Luján, F. E. López Monteagudo, J. De La Torre y Ramos, and L. del C. R. Rodríguez, "Characterization of a Low Power Wind Turbine Prototype for Interconnection to the Grid," Journal of Engineering and Technology for Industrial Applications (ITEGAM-JETIA), vol. 10, no. 46, pp. 22-26, Mar./Apr. 2024. . [Online]. Available: https://doi.org/10.5935/jetia.v10i46.1110

[15] A. G. Abubakar and M. R. Khan, "Artificial Neural Network-based control for enhanced MPPT in wind energy systems," Renewable Energy, vol. 159, pp. 173–186, 2020. [Online]. Available: https://doi.org/10.1016/j.renene.2020.06.147

[16] H. H. Alhelou, M. M. Khan, and S. Sun, "A survey on ANN applications in renewable energy systems: Case studies for wind energy," IEEE Access, vol. 8, pp. 108456–108469, 2020. [Online]. Available: https://doi.org/10.1109/ACCESS.2020.3000768

[17] K. Al-Haddad and M. Krishnan, "Lyapunov-based backstepping for stability enhancement in wind energy conversion systems," International Journal of Electrical Power & Energy Systems, vol. 122, pp. 106177, 2020. [Online]. Available: https://doi.org/10.1016/j.ijepes.2020.106177

[18] E. M. Youness, A. Derouich, A. E. Ghzizal, J. Bouchnaif, N. E. Ouanjli, O. Zamzoum, K. Mezioui, and B. Bossoufi, "Implementation and validation of backstepping control for PMSG wind turbine using dSPACE controller board," Energy Reports, vol. 5, pp. 807-821, 2019. [Online]. Available: https://doi.org/10.1016/j.egyr.2019.06.001.

[19] B. Majout, B. Bossoufi, M. Karim, P. Skruch, S. Mobayen, Y. El Mourabit, and Z. El Zair Laggoune, "Artificial neural network-based direct power control to enhance the performance of a PMSG-wind energy conversion system under real wind speed and parameter uncertainties: An experimental validation," Energy Rep., [Online]. Available: https://doi.org/10.1016/j.egyr.2023.06.015

[20] M. W. Khan, J. Wang, L. Xiong, and M. Ma, "Fractional order sliding mode control of PMSG-wind turbine exploiting clean energy resource," International Journal of Renewable Energy Development, vol. 8, no. 1, pp. 81–89, 2019. [Online]. Available: https://doi.org/10.14710/ijred.8.1.81-89

[21] H. Chojaa, A. Derouich, S. E. Chehaidia, O. Zamzoum, M. Taoussi, and H. Elouatouat, "Integral sliding mode control for DFIG-based WECS with MPPT based on artificial neural network under a real wind profile," Energy Reports, vol. 7, pp. 4809–4824, 2021. [Online]. Available: https://doi.org/10.1016/j.egyr.2021.07.066

[22] I. U. Khan, L. Khan, Q. Khan, S. Ullah, U. Khan, and S. Ahmad, "Neuro-adaptive backstepping integral sliding mode control design for nonlinear wind energy conversion system," Turkish Journal of Electrical Engineering & Computer Sciences, vol. 29, no. 2, pp. 531–547, 2021. [Online]. Available: https://doi.org/10.3906/elk-2001-113

[23] E. Mahersi and A. Khedher, "Backstepping flux observer for nonlinear control of the direct-drive permanent magnet synchronous generator wind turbines," Wind Engineering, vol. 40, pp. 540–554, 2016. [Online]. Available: https://doi.org/10.1177/0309524X16658519

[24] G. Xue, F. Lin, S. Li, and H. Liu, "Adaptive fuzzy finite-time backstepping control of fractional-order nonlinear systems with actuator faults via command-filtering and sliding mode technique," Information Sciences, vol. 600, pp. 189–208, 2022. [Online]. Available: https://doi.org/10.1016/j.ins.2022.02.052

[25] F. Wang, Y. Guo, K. Wang, Z. Zhang, C. Hua, and Q. Zong, "Disturbance observer based robust backstepping control design of flexible air-breathing hypersonic vehicle," IET Control Theory and Applications, vol. 13, pp. 572–583, 2019. [Online]. Available: https://doi.org/10.1049/iet-cta.2018.5480

[26] Y. El Mourabit, H. Salime, B. Bousouf, S. Motahhir, A. Derouich, S. Mobayen, and A. Zhilenkov, "Enhanced Performance in PMSG-Based Wind Turbine Systems: Experimental Validation of Adaptive Backstepping Control Design," Energies, vol. 16, no. 8, p. 3880, 2023. [Online]. Available: https://doi.org/10.3390/en16083880

[27] Y. Mousavi, G. Bevan, I. B. Kucukdemiral, and A. Fekih, "Sliding mode control of wind energy conversion systems: Trends and applications," *Renewable and Sustainable Energy Reviews,* vol. 167, Art. no. 112734, Oct. 2022. [Online]. Available: https://doi.org/10.1016/j.rser.2022.112734

[28] A. Poovathody and R. Ramchand, "Twelve Sector Based Direct Power Control of Induction Motor Drives," 2020 International Conference on Power Electronics and Renewable Energy Applications (PEREA), Nov. 2020, pp. 1–5. [Online]. Available: https://doi.org/10.1109/PEREA51218.2020.9339794

[29] A. Jain, J. Singh, S. Kumar, T. Florin-Emilian, M. Traian Candin, and P. Chithaluru, "Improved recurrent neural network schema for validating digital signatures in VANET," Mathematics, vol. 10, no. 20, p. 3895, 2022. [Online]. Available: https://doi.org/10.3390/math10203895

[30] B. N. Kommula and V. R. Kota, "An effective sustainable control of brushless DC motor using firefly algorithm – Artificial neural network based FOPID controller," Sustainable Energy Technologies and Assessments, vol. 52(B), p. 102097, 2022. [Online]. Available: https://doi.org/10.1016/j.seta.2022.102097.

[31] I. Saady, M. Karim, B. Bossoufi, N. El Ouanjli, S. Motahhir, and B. Majout, "Optimization and control of photovoltaic water pumping system using Kalman filter-based MPPT and multilevel inverter fed DTC-IM," *Results in Engineering*, vol. 17, Art. no. 100829, Mar. 2023. [Online]. Available: https://doi.org/10.1016/j.rineng.2022.100829.

[32] A. Kasri and K. Ouari, "Robust Intelligent Nonlinear Predictive Control Based on Artificial Neural Network for Optimizing PMSM Drive Performance," *Periodica Polytechnica Electrical Engineering and Computer Science*, vol. 68, no. 4, pp. 356–366, Sep. 2024. [Online]. Available: https://doi.org/10.3311/PPee.37217.